ChemPubSoc Europe

DOI: 10.1002/chem.201705748

CHEMISTRY A European Journal Full Paper

Ab Initio Calculations |*Hot Paper*|

Crystal Field in Rare-Earth Complexes: From Electrostatics to Bonding

Riccardo Alessandri,[a, b] Habiburrahman Zulfikri,[a, c] Jochen Autschbach,[d] and Hélène Bolvin*[a, e]

Abstract: The flexibility of first-principles (ab initio) calculations with the SO-CASSCF (complete active space self-consistent field theory with a treatment of the spin-orbit (SO) coupling by state interaction) method is used to quantify the electrostatic and covalent contributions to crystal field parameters. Two types of systems are chosen for illustration: 1) The ionic and experimentally well-characterized $PrCl_3$ crystal; this study permits a revisitation of the partition of contributions proposed in the early days of crystal field theory; and 2) a series of sandwich molecules $[Ln(\eta^n\text{-}C_nH_n)_2]^q$, with Ln = Dy, Ho, Er, and Tm and $n = 5$, 6, and 8, in which the interaction between Ln^{III} and the aromatic ligands is more difficult to describe within an electrostatic approach. It is shown that a model with three layers of charges reproduces the electrostatic field generated by the ligands and that the covalency plays a qualitative role. The one-electron character of crystal field theory is discussed and shown to be valuable, although it is not completely quantitative. This permits a reduction of the many-electron problem to a discussion of the energy of the seven 4f orbitals.

Introduction

Crystal field theory (CFT) is fundamental for those who deal with 4f–4f transitions and magnetic properties of lanthanide (Ln) elements and their complexes.[1] CFT describes the splitting of metal orbitals, either d or f, by the static electrostatic field created by the ligands described as a charge distribution. This approach was first proposed in the 1930s by Bethe[2] and Van Vleck[3] and CFT became more tractable during the 1950s thanks to the works of Racah[4] and Stevens,[5] who applied the Wigner–Eckart theorem to simplify the evaluation of the crystal field (CF) matrix elements for many-electron cases. These crystal field parameters (CFPs) could be determined from optical spectra.[6] The limitations of the purely electrostatic picture underlying CFT were demonstrated in the 1950s for the d elements (transition metals). CFT was eventually supplanted by ligand field theory, which treats bonding between the metal ion and the ligands within a molecular orbital framework.[7,8] Overlap between the d orbitals of transition metals and those of the ligands is much larger than that for the 4f orbitals of the lanthanides because the latter are radially very compact, and the Ln 4f shells are screened from the external field of the ligands by the filled $5s^25p^6$ shells.

From the very beginning it was established that CFT provided a theoretical framework that permitted the parametrization of the ion environment by means of few parameters and that CFPs were phenomenological and should thus be fitted on experimental data, but the purely electrostatic model was not able to predict their values. Although the electrostatic approach clearly fails for the d elements, CFT remains a commonly used method to study the properties of open-shell lanthanides.

With the discovery of lanthanides as single-ion magnets, there has been a resurgence in synthetic activity to develop new lanthanide complexes. CFT is widely used to rationalize the properties of these complexes, in particular, the nature of the ground state and the anisotropic magnetic properties. Two programs, CONDON and PHI, have been developed for efficient fitting of the CFPs to experimental data.[9,10] On an electrostatic basis, Rinehart and Long showed that an oblate or prolate shape of the ligand environment favored greater stability of one or another M_J component of the metal-ion ground level.[11] Computational models based on electrostatic approaches have been recently proposed, based on either a combined electro-

[a] *R. Alessandri, H. Zulfikri, Dr. H. Bolvin*
Laboratoire de Chimie et Physique Quantiques, CNRS
Université Toulouse III, 118 route de Narbonne, 31062 Toulouse (France)
E-mail: bolvin@irsamc.ups-tlse.fr

[b] *R. Alessandri*
Present address: Zernike Institute for Advanced Materials and
Groningen Biomolecular Sciences and Biotechnology Institute
University of Groningen, Nijenborgh 4, 9747 AG
Groningen (The Netherlands)

[c] *H. Zulfikri*
Present address: MESA + Institute for Nanotechnology
University of Twente, P.O. Box 217, 7500 AE Enschede (The Netherlands)

[d] *Prof. Dr. J. Autschbach*
Department of Chemistry, University at Buffalo
State University of New York, Buffalo, NY 14260-3000 (USA)

[e] *Dr. H. Bolvin*
On research leave for the period August 2017 to June 2018
Temporary address: Hylleraas Center for Quantum Molecular Sciences
Department of Chemistry, University of Oslo, Oslo (Norway)

Supporting information and the ORCID numbers for the authors of this article can be found under https://doi.org/10.1002/chem.201705748.

static description with the semiempirical radial effective charges (REC) approach[12] or a description of the ligands by charges optimized to fit the experimental data in the lone pair effective charge (LPEC) approach. In the case of aromatic ligands, it is necessary to add more parameters (a displacement parameter) to mimic the covalency.[13] A purely electrostatic approach has been proposed to determine the direction of the magnetic moment, by minimizing the potential energy; the ligands are modeled by fractional charges determined by valence-bond resonance hybrids.[14] First-principles calculations are regularly used to quantify the degree of covalency in metal–ligand bonding.[15–19] CFPs may be deduced from first-principles methods and the contribution of covalency to CFPs was recently confirmed to be non-negligible.[20,21]

The first-principles method SO-CASSCF (complete active space self-consistent field theory with a treatment of the spin-orbit (SO) coupling by state interaction) has shown its capability, in many cases, to reproduce the magnetic data of the complexes, and give further physical insights, especially regarding the nature of the ground and excited states, into the direction of the magnetic moment and the energetic spectrum and chemical bonding. Herein, we use SO-CASSCF calculations to check the validity of some assumptions behind CFT, such as the one-electron approach and the purely electrostatic model. The two considered molecular systems are symmetrical, so that they have few CFPs: 1) The ionic crystal $PrCl_3$, which is fully characterized experimentally and has served as a test for improvements to the theory since the early days of CFT; thanks to its high symmetry, only four CFPs are sufficient to describe its full CF spectrum; and 2) a series of model sandwich complexes of high symmetry, in which the aromatic ligands form covalent bonds with the metal ion: $[Ln(\eta^5\text{-}C_5H_5)_2]^+$ (**LnCp**), $[Ln(\eta^6\text{-}C_6H_6)_2]^{3+}$ (**LnBz**), and $[Ln(\eta^8\text{-}C_8H_8)_2]^-$ (**LnCOT**), in which Ln = Dy, Ho, Er, and Tm are considered. First, the many-electron problem is reduced to the discussion of the energetic ordering of the 4f orbitals, and then the two model systems are considered.

Results and Discussion

CFT: From orbitals to many-electron states

Magnetic properties of rare-earth complexes may be described by the splitting of the $2J+1$ manifold, which arises from the term of the free ion, $^{2J+1}L_J$, by the ligands. This effect was first calculated to be the electrostatic interaction of the f electrons with the ligands described by point charges.[2] In this approach, the electrostatic potential at point r close to the magnetic center is written as a multipolar expansion [Eq. (1)]:

$$v^{CF}(r) = \sum_{k=0}^{\infty}\sum_{q=-k}^{k} B_k^q r^k Y_k^q(\theta,\phi) = \sum_{k,q} V_k^q \qquad (1)$$

in which $\boldsymbol{r}$ is expressed by using the spherical coordinates around this ion (r,θ,ϕ), and Y_k^q are spherical harmonics. The many-electron wavefunctions of a $4f^N$ ion may be written as linear combinations of Slater determinants, $|\phi_i \cdots \phi_j|$, built with 4f spin-orbitals, ϕ_i, in which the occupied spin orbitals of the closed shells have been omitted. The CF operator is the sum of the one-electron operators [Eq. (2)]:

$$V^{CF} = \sum_{i=1}^{N} v^{CF}(r_i) \qquad (2)$$

V_k^q is a component of an irreducible tensor, and matrix elements within a given f^N configuration vanish for $k>6$, as well as for odd values of k. The first term, with $k=0$, does not produce any CF splitting. The noncontributing terms (k,q) are usually omitted in the expansion of Equation (2). The number of terms is further reduced by the symmetry of the surrounding crystal.

Assuming that all 4f orbitals have the same spatial expansion, the V_k^q operators acting in the Hilbert space of the Slater determinants may be replaced by the equivalent operators O_k^q acting in either the l, L, or J manifolds. Equation (2) is then equivalent to Equation (3):

$$\hat{V}^{CF}(X) = \alpha_X \sum_{q=-2}^{2} B_2^q \hat{O}_2^q(X) + \beta_X \sum_{q=-4}^{4} B_4^q \hat{O}_4^q(X) + \gamma_X \sum_{q=-6}^{6} B_6^q \hat{O}_6^q(X) \qquad (3)$$

in which $X=l$, L, or K, according to the considered manifold. $\eta_X = \langle X\|\eta\|X\rangle$, $\eta = \alpha,\beta,\gamma$ are the reduced matrix elements of second, fourth, and sixth order, respectively. η_l are determined by N, η_L by N and L and η_J by N, L, and J and are tabulated for the ground states of the Ln series.[22]

Equation (3) is deduced from a purely electrostatic model, in which each 4 f electron of the magnetic center is supposed to move independently in the electrostatic field of the charges representing the ligands. It was observed very early that the modeling of ligands by point charges was not sufficient and, in the 1960s, CFT improved with the use of more sophisticated descriptions of the ligand sphere by including dipole and quadrupole moments to describe the effect of the ligands[23–25] and by adding polarization charges on the ligands.[26] Screening of the filled $5s^25p^6$ shells, which lie outside the open-shell $4f^n$ has been considered,[27–29] and models beyond the one-electron picture have been proposed by introducing the effect of configuration interactions.[30,31] The role of covalency was noted very early, although it is not as large as that for transition metals and several methods have been proposed to include covalent effects for lanthanides after the success of ligand field theory in d complexes.[32–34] Two widely used semiempirical approaches to describe the ligands by parameters based on overlap have been developed: the angular overlap model (AOM)[35] and superposition methods.[1,36] In the models based on ligand field theory, the Hamiltonian is still a one-electron operator, so the form of Equation (3) is maintained. Equation (3) is used and the parameters are fitted to experimental data. As such, CFT serves for the parametrization of the environment by means of a few parameters, which can be kept

small, in particular, for high-symmetry environments. CFT is by its nature rooted in a one-electron picture. Some attempts have been made to consider two-electron terms, but this leads to too large a number of parameters for subsequent fitting.

The many-electron wave function is written as shown in Equation (4), by omitting the closed-shell electrons:

$$\Psi_M = \sum_I C_I^M \underbrace{\left|f_i \cdots f_j \bar{f}_{i'} \cdots \bar{f}_{j'}\right|}_{N} \tag{4}$$

The corresponding population of orbital f_m is given by Equation (5):

$$\rho_m^M = \left\langle \Psi_M \middle| \hat{N}_m \middle| \Psi_M \right\rangle \tag{5}$$

in which $\hat{N}_m$ is the number operator. In a pure *LS* coupling scheme, first the $|L, M_L, S, M_S\rangle$ state is obtained by coupling *N* one-electron angular momenta, $l_1 \otimes \cdots \otimes l_N$, and the many-electron wave function is built according to Clebsch–Gordan coefficients. Then, the $|J, M_J\rangle$ states are built by $L \otimes S$ coupling, again with the Clebsch–Gordan coefficients. It follows that, given *N* 4f electrons, the values of *L*, *S*, and *J* are determined by the three Hund rules and the population of a given f_m orbital is fully determined. The $\rho_m^{M_L}$ values deduced from *LS* coupling for Dy^{III} and Tm^{III} ions are compared in Table 1 to the spin-free (SF)-CASSCF values for **LnCp** and **LnCOT** (the structures of which are represented in Figure 3, below). The *LS* coupling populations are close to those of the SF-CASSCF calculations; they are essentially identical for the largest values of M_L and remain close to each other even for the lowest M_L, for which the wave functions become more multiconfigurational.

The energies of the 4f orbitals, as shown in Figure 1, depend predominantly on the ligand, and only very weakly on the metal and number of 4f electrons. A discussion on the ordering of the orbitals is provided in the last section for the sandwich complexes. In Table 1, the ab initio occupancies of

Table 1. Population of f_m orbitals in the $|L, M_L\rangle$ state $\rho_m^{M_L}$ [see Eq. (5)] calculated by *LS* coupling (in italics) and deduced from SO-CASSCF calculations for **LnCp** and **LnCOT** (Ln = Dy, Tm; $L = 5$). The model function is defined as $|f_i f_j|$; for Dy, it corresponds to $|f_3 f_2 f_1 f_0 f_{-1} f_{-2} f_{-3} \bar{f}_3 \bar{f}_2 \bar{f}_1 \bar{f}_0 \bar{f}_{-1} \bar{f}_{-2} \bar{f}_{-3}|$ and for Tm, to two holes in $|f_3 f_2 f_1 f_0 f_{-1} f_{-2} f_{-3} \bar{f}_3 \bar{f}_2 \bar{f}_1 \bar{f}_0 \bar{f}_{-1} \bar{f}_{-2} \bar{f}_{-3}|$.

M_L	wf	Dy				Tm			
		f_0	$f_{\pm1}$	$f_{\pm2}$	$f_{\pm3}$	f_0	$f_{\pm1}$	$f_{\pm2}$	$f_{\pm3}$
5	$\|f_3 f_2\|$	*1*	*2*	*3*	*3*	*2*	*4*	*3*	*3*
	LnCOT	1.00	2.00	3.00	3.00	2.00	4.00	3.00	3.00
	LnCp	1.00	2.00	3.00	3.00	2.00	4.00	3.00	3.00
4	$\|f_3 f_1\|$	*1*	*3*	*2*	*3*	*2*	*3*	*4*	*3*
	LnCOT	1.00	2.99	2.00	2.99	2.00	3.00	4.00	3.00
	LnCp	1.00	3.00	2.00	3.00	2.00	3.00	4.00	3.00
3	$(\sqrt{2}\|f_3 f_0\| + \|f_2 f_1\|)/\sqrt{3}$	*1.66*	*2.33*	*2.33*	*2.66*	*1.33*	*3.66*	*3.66*	*3.33*
	LnCOT	1.69	2.30	2.30	2.69	1.35	3.64	3.64	3.35
	LnCp	1.73	2.27	2.27	2.73	1.38	3.61	3.61	3.38
2	$(\sqrt{2}\|f_2 f_0\| + \|f_3 f_{-1}\|)/\sqrt{3}$	*1.66*	*2.33*	*2.66*	*2.33*	*1.33*	*3.66*	*3.33*	*3.66*
	LnCOT	1.66	2.34	2.66	2.34	1.33	3.67	3.33	3.67
	LnCp	1.64	2.36	2.64	2.36	1.31	3.69	3.31	3.69
1	$(\sqrt{10}\|f_1 f_0\| + 3\sqrt{3}\|f_2 f_{-1}\| + \sqrt{5}\|f_3 f_{-2}\|)/\sqrt{42}$	*1.24*	*2.88*	*2.76*	*2.11*	*1.76*	*3.12*	*3.24*	*3.88*
	LnCOT	1.28	2.91	2.72	2.08	1.79	3.14	3.21	3.85
	LnCp	1.18	2.82	2.81	2.18	1.72	3.08	3.27	3.91
0	$(5\|f_1 f_{-1}\| + 4\|f_2 f_{-2}\| + \|f_3 f_{-3}\|)/\sqrt{42}$	*1*	*3.19*	*2.76*	*2.05*	*2*	*2.81*	*3.24*	*3.95*
	LnCOT	1.00	3.34	2.63	2.02	2.00	2.95	3.12	3.93
	LnCp	1.00	2.91	2.97	2.11	2.00	2.65	3.37	3.98

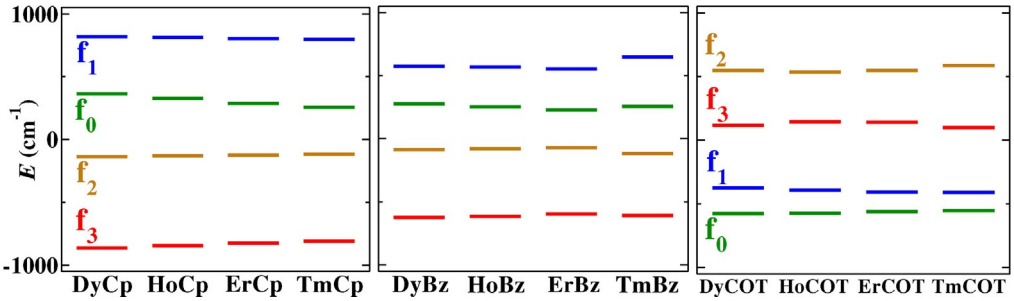

Figure 1. CASSCF canonical energies of 4f orbitals for **LnCp**, **LnBz**, and **LnCOT** complexes. Orbitals are labeled and colored after $|m_l|$ and zero is taken as the average of the seven energies.

the lowest energy orbitals are slightly larger than those of the model, but slightly smaller for the highest orbitals. Splitting of the 4f orbitals is less than 2000 cm^{-1}. A large splitting favors the Aufbau principle. However, in the case of the lanthanides, the splitting is small enough that Hund's rules for the free ion still apply. Consequently, splitting of the 4f orbitals barely impacts on their occupancy, relative to those deduced from the *LS* coupling scheme for the free ion. In an independent electron picture, the energy of the many-electron wave function is deduced from the orbital energies as given by Equation (6):

$$E_M = \sum_{m=-3}^{3} \rho_m^M \varepsilon_m \qquad (6)$$

in which ε_m is the energy of the f_m orbital. The energies deduced from Equation (6) with the population of the free-ion and the canonical energies for the given complex are compared with those obtained by SF-CASSCF in Figure 2. It should be noted that applying Equation (6) with canonical orbitals energies implies a double counting of the electron–electron repulsion energies, but, since we consider only differences in energies and because repulsion between the different 4f orbitals is roughly the same, it should not impact on the results. Figure 2 demonstrates that the ordering of the whole spectrum is correct, except that the $|M_L| = 5$ states of **TmCOT** are wrongly positioned. This shows that the energies of the $2J+1$ lowest states of a lanthanide complex are to a large degree determined by the energetic ordering of the 4f orbitals, in accordance with the one-electron structure of CFT.

A Hamiltonian describing the f electrons may be written as Equation (7):

$$\hat{\mathcal{H}}_{CF} = \sum_{i=1}^{N}\left[-\frac{1}{2}\hat{T}_i^2 - \frac{Z^*}{r_i}\right] + \sum_{i<j}\frac{1}{r_{ij}} + \sum_{i=1}^{N}\left(\xi\hat{l}_i \cdot \hat{s}_i + \hat{V}_{CF}(i)\right) \qquad (7)$$

with a scalar relativistic kinetic term $\hat{T}$, the screened charge of the nucleus Z*, the electron–electron repulsion, the spin–orbit coupling (SOC) operator, and the CF operator of Equation (1). Equation (3) may be applied in the *l*, *L*, or *J* spaces. We may extract the CFPs from three levels of calculation: 1) From the splitting of the orbitals; the CFPs are deduced from the energies of the canonical orbitals with $l=3$. This step corresponds to neglecting the residual Coulomb interaction above the one-electron central field operator and the SOC in Equation (7). 2) From the SF-CASSCF calculations, which provide many-electron states without SOC. The CFPs are calculated within the $2L+1$ manifold, in which *L* is the orbital quantum number of the free ion and should correspond to the model Hamiltonian of Equation (7) without the SOC term. 3) From the SO-CASSCF calculations, which provide many-electron wave functions including SOC. The CFPs are calculated in the $2J+1$ manifold and include all of the physics of Equation (7). These different CFPs are compared for some sandwich complexes in Table 2

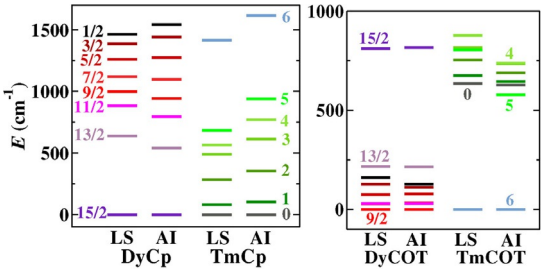

Figure 2. Energies of the $2J+1$ manifold determined by Equation (6) (*LS*) and SO-CASSCF calculations (AI) for **DyCp**, **TmCp**, **DyCOT**, and **TmCOT**. Zero is taken as the ground state. The states are labeled and colored after $|M_J|$.

Table 2. CFPs [cm^{-1}] fitted on the $2l+1$ orbital, $2L+1$ SF-CASSCF, and $2J+1$ SO-CASSCF energies for **LnCp**, **LnBz**, and **LnCOT** (Ln = Dy, Tm).

		Dy			Tm		
		$l=3$	$L=5$	$J=152$	$l=3$	$L=5$	$J=6$
LnCp	B_2^0	1339	1276	1301	1245	1306	1307
	B_4^0	15	43	22	−2	15	20
	B_6^0	−100	−79	−68	−108	−74	−76
LnBz	B_2^0	966	941	950	887	942	943
	B_4^0	7	24	14	−7	10	13
	B_6^0	−67	−55	−50	−68	−46	−47
LnCOT	B_2^0	−511	−550	−498	−504	−530	−542
	B_4^0	−299	−273	−280	−314	−222	−218
	B_6^0	35	29	38	46	19	18

and for $PrCl_3$ in Table 4, below. They are qualitatively the same; those issued from SF-CASSCF and SO-CASSCF energies are more similar than those issued from orbital energies. This means that the building of the many-electron wave function has a greater effect on CFPs than that of calculating the SOC.

CFPs in $PrCl_3$

$PrCl_3$ is an ionic solid that crystallizes in the $P6_3/m$ space group.[37,38] The Pr^{III} ion is surrounded by nine approximately equidistant nearest Cl^- anions, leading to a point group symmetry for the Pr^{III} ion of D_{3h}. Three of the ligands are coplanar, with the Pr^{III} ion at a distance of 2.911 Å. Of the other six ligands, three lie in a parallel plane above and three below; all at a distance of 2.902 Å from the Pr^{III} ion (see Figure 3). In the following, the $[PrCl_9]^{6-}$ cluster is considered. In D_{3h} symmetry, Equation (3) reduces to Equation (8):

$$\hat{V}_{D_{3h}}^{CF}(X) = \alpha_X B_2^0 \hat{O}_2^0(X) + \beta_X B_4^0 \hat{O}_4^0(X) + \gamma_X\left[B_6^0 \hat{O}_6^0(X) + B_6^6 \hat{O}_6^6(X)\right] \qquad (8)$$

with $X = l$, *L*, and *J* and the quantification axis along the C_3 axis. The ground term of the Pr^{III} free ion is $^3H_4$. Because there are only four CFPs, they are easily deduced from energy spectra. The 4f orbitals ($l=3$) split into five levels, without SOC, the $L=5$ term splits into seven levels, and the SO $J=4$ term splits into six levels (see Table 3). The B_6^6 term results in coupling between components with $\Delta M = \pm 6$.

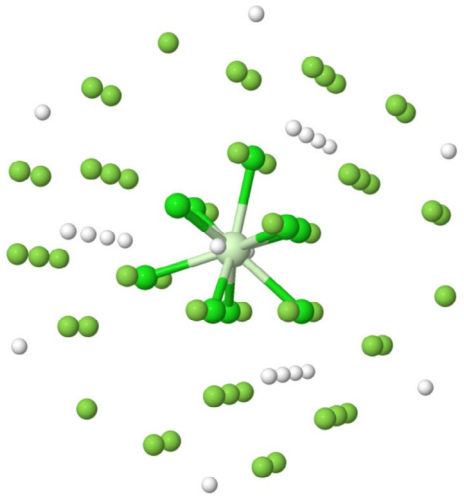

Figure 3. Structure of the $PrCl_3$ crystal. The atoms of the $[PrCl_9]^{6-}$ cluster are represented with larger radii. White: Pr, green: Cl.

Table 3. Splitting of the different terms according to the m_l, M_L, and M_J values in D_{3h} symmetry. The degeneracy of the levels is given in parentheses.

$l=3$	$L=5$	$J=4$
0 (1)	0 (1)	0 (1)
±1 (2)	±1, ∓5 (2)	±1 (2)
±2 (2)	±1, ∓5 (2)	±2, ∓4 (2)
±3 (1)	±2, ∓4 (2)	±2, ∓4 (2)
±3 (1)	±2, ∓4 (2)	±3 (1)
	±3 (1)	±3 (1)
	±3 (1)	

$PrCl_3$ has been extensively studied, both experimentally and theoretically, and has served as a test for all developments of CFT. The optical absorption of Pr^{III} substituted at La^{III} sites in the isomorph $LaCl_3$ crystal was studied by Sayre et al.,[39] who performed the first evaluation of the CFPs. Hutchison and Wong probed the ground state of this substituted crystal by EPR spectroscopy and determined the g factors: $g_{\|}=1.035\pm0.005$ and $g_{\perp}=0.1\pm0.15$.[40] Combined with the optical spectrum, they proposed CFPs that had been refined by more accurate calculations (Table 4).[41,42] Sayre et al.[39] recorded the absorption and fluorescence spectra at the temperature of helium and deduced the energy and nature of the low-lying spectrum[43] (Table 5).

The theoretical determination of the CFPs has been performed by different methods. Hutchings and Ray showed that the point-charge model was inadequate, and improved it by evaluating the contribution of induced dipoles and quadrupoles, but there were still large discrepancies between calculated and experimental values.[23] The electrostatic model has been refined by adding the polarizability of the metal ion[24] and refining the charge distribution on the ligands.[25] Finally, covalency was introduced by means of the superposition model[44–47] or by covalent parameters.[33] It was pointed out that these covalency models were more interpretative than predictive. Finally, the CFPs have been deduced from $X\alpha$ calculations.[48] Newman partitioned all effects according to 10 distinct contributions in Table 12 in reference [1].

Herein, the $PrCl_3$ crystal is described at different levels to build up the environment step by step: 1) The pure CF level, in which the 4f orbitals are placed in the electrostatic potential of nine point charges, $Q=-1$, at the position of the chloride anions (labeled CF). 2) The CASSCF calculation of a Pr^{III} cation described with a basis set, either minimal (MB) or triple-ζ polarized (TZP), and the Cl^- anions are described by either a point charge, $Q=-1$, or an effective core potential (ECP) without any basis set with $Q=-1$. The latter description avoids the penetration of the electrons of the Pr^{III} cation into the ionic radius of the anions. 3) The $[PrCl_9]^{6-}$ cluster is described with a full basis set of TZP quality. 4) The full $[PrCl_9]^{6-}$ cluster is embedded in a set of point charges within a radius of 8 Å to represent the long-range electrostatic interactions within the crystal.

CFPs are evaluated from 4f canonical ($l=3$), SF-CASSCF ($L=5$), and SO-CASSCF ($J=4$) energies, as summarized in Table 4. For a given level of calculation, the l, L, and J CFPs differ only by a few cm^{-1}. This confirms that the one-electron theory is suitable for this ionic system. Adding a MB basis set on Pr^{3+} reduces only B_2^0, compared with the CF values, due to screening from the occupied 5s and 5p shells, which lie out of the 4f shell. With a larger basis set, all CFPs are strongly reduced, which leads to a global reduction of about 40% of all CFPs; a larger basis set gives better flexibility to describe polarization and allows the electron density of the cation to better avoid the negative potential in the environment, in particular, CFPs in the order of four and six. The addition of pseudopotentials at the chlorine positions has little effect. Treating the chlorine ligands quantum mechanically (TZP), however, has a large effect and gives CFPs very close to those of the experimental

Table 4. CFPs [cm^{-1}] of $PrCl_3$ deduced from different types of calculations.

Pr	CF		MB			TZP			TZP			TZP			TZP			Exptl[a]
Cl	$q=-1$		$q=-1$			$q=-1$			ECP $=-1$			TZP			TZP + emb			
	$l=3$	$l=3$	$L=5$	$J=4$	$l=3$	$L=5$	$J=4$	$l=3$	$L=5$	$J=4$	$l=3$	$L=5$	$J=4$	$l=3$	$L=5$	$J=4$	
B_2^0	196.2	153.9	147.0	146.6	105.9	105.1	104.4	107.3	106.1	105.5	45.3	48.4	46.5	28.9	24.2	30.0	47.2
B_4^0	−27.4	−28.6	−28.7	−28.8	−17.6	−19.5	−19.2	−14.3	−16.0	−15.9	−30.0	−32.3	−29.0	−39.7	−41.7	−41.7	−40.5
B_6^0	−5.7	−4.9	−5.5	−5.7	−2.6	−3.0	−3.0	−2.6	−3.32	−3.3	−28.2	−26.4	−27.1	−43.2	−42.7	−42.9	−39.6
B_6^6	−69.4	58.4	65.8	63.7	31.6	35.8	34.9	31.5	40.3	39.4	340.0	336.1	341.1	397.8	398.0	413.5	405.4

[a] Reference [42].

Table 5. $PrCl_3$ electronic energies [cm^{-1}] and degeneracies (in parentheses) of the states with $^3H_4$ ion parentage. Ground doublet composition and $g_{\|}$.

Pr Cl	MB $q=-1$	TZP $q=-1$	TZP ECP-1	TZP[a] TZP	TZP[b] TZP	TZP[a] TZP + emb	TZP[b] TZP + emb	Fitted CFPs[c]	Exptl[d]
$E_{\pm4/\mp2}(2)$	0	0	0	0	0	0	0	0	0
$E_{\pm3}(1)$	20.4	16.2	21.7	24.9	18.4	56.4	45.2	33.2	33.1
$E_{\pm2/\mp4}(2)$	72.7	54.0	58.3	84.7	74.5	125.	111.6	97.9	96.4
$E_{\pm1}(2)$	134.4	95.5	97.5	101.6	93.2	130.	118.2	131.3	130.2
$E_{\pm3}(1)$	40.0	27.0	33.8	132.1	111.9	185.5	158.0	142.3	137.0
$E_0(1)$	164.2	114.7	115.8	163.0	148.9	223.	202.9	210.0	–
$g_{\|}$	6.24	6.34	6.34	0.60	0.64	1.76	1.86	0.98	1.035
α^2[e] [%]	99	99	99	27	26	14	13	23	

[a] SOC limited to triplets. [b] SOC including both triplets and singlets. [c] Ref. [42]. [d] Refs. [39,40]. [e] The ground-state doublet is written as $\alpha|\pm4\rangle+\beta|\mp2\rangle$.

values. B_2^0 decreases by half, whereas B_6^6 increases by an order of magnitude. In other words, if the partial covalency of the metal–ligand interactions is taken into account, the purely electrostatic description, which mimics bonding, becomes more anisotropic. Finally, with the point charges added to describe the Madelung field of the crystal, the calculated CFPs are even closer to those derived from experimental data, with the exception of B_2^0.

The energies of the 4f orbitals for different environments are shown in the Supporting Information. The electrostatic fields generated by the three equatorial chlorine atoms, on one hand, and by the six nonequatorial chlorine atoms, on the other hand, are opposite, about 1000 cm^{-1}, and partly compensate for each other. Covalency impacts on the splittings and is due to both σ and π interactions. The rather small splitting of the 4f orbitals (300 cm^{-1}) is due to the geometrical arrangement of the ligands close to spherical symmetry.

The state energies and $g_{\|}$ factor for the ground doublet are given in Table 5 and compared with the experimental values. Due to B_6^6, which originates essentially from covalency and splits the two $|M_J\rangle=|\pm3\rangle$ states, ordering of the states is only achieved with the quantum mechanical description of the ligands. The ground state is a mixture of $\alpha|\pm2\rangle+\beta|\mp4\rangle$, the weights of which depend strongly on the level of calculation. Pure $|\pm4\rangle$ in the electrostatic model, becomes mostly $|\pm2\rangle$ with covalency. The corresponding $g_{\|}=2g_J|4\alpha^2-2\beta^2|$ (with $g_J=4/5$ for $^3H_4$) term is very sensitive to the state composition; the composition without embedding is in better agreement with the experimental one than that with embedding. The sensibility of the *g* factors has already been observed in the case of states mixing.[49]

This study is in accordance with the previous partition summarized by Newman in Table 12 of reference [1], even if our partitioning is not exactly the same. This step by step first-principles approach shows that shielding by the external electron density of the cation and polarization reduces the electrostatic interaction between 4f and the ligands by about 40% and the covalency plays a quantitative role, especially on B_6^6.

To conclude this section, our study shows that, although $PrCl_3$ is an ionic crystal, a purely electrostatic description of the ligands is only qualitative. To obtain a quantitative description, the covalent interactions between the metal and ligands must be treated.

CFPs in $[Ln(\eta^n\text{-}C_nH_n)_2]^q$

In this section, we consider a series of lanthanide sandwich complexes with cyclopentadienide (Cp^-), benzene (Bz), and cyclooctatetraenide (COT^{2-}) ligands. These complexes were chosen because 1) of their axial symmetry, which reduces the number of CFPs; 2) the ligands are aromatic and their description by point charges is not trivial; and 3) the covalency between the metal and ligands is important. Complexes **LnCp** and **LnBz** are in the staggered configuration, whereas **LnCOT** is eclipsed, leading to D_{5d}, D_{6d}, and D_{8h} point groups, respectively (see Figure 4).

Although one finds many lanthanide complexes with Cp^-, Bz, and COT^{2-} ligands,[50] there is no experimental evidence for either **LnCp** or **LnBz**. Cp^- is usually found in a tris-coordination mode as derivatives of $[Ln(\eta^5\text{-}Cp)_3]$[51] or in bis-coordination with another ligand, $[Ln(\eta^5\text{-}Cp)_2L]$. The neutral form, $[Ln(\eta^5\text{-}C_5Me_5)_2]$, has been characterized and described theoretically.[52] With Bz, the zero-valent sandwich $[Ln(\eta^6\text{-tri-}t\text{BuBz})_2]$ is known;[53] the unsubstituted form, $[Ln(\eta^6\text{-}C_6H_6)_2]$, has been theoretically described;[54] and monocoordinated $[Ln(\eta^6\text{-}C_6H_6)]$ has been characterized.[55,56] On the contrary, there are many examples of sandwich ligands of the type $[Ln(\eta^8\text{-}C_8H_8)_2]^-$ with different substituted forms of the ligands.[57–59] Due to the steric bulk of the ligands, all of these molecules are tilted. The **LnCOT** complexes have been described by various theoretical methods,[60–63] and the full series has been recently described by the CASSCF method.[64] Some of these complexes show single-molecule magnet behavior.[59,65–67]

Figure 4. Equilibrium geometries of the sandwich complexes.

The Ln–ligand distances optimized with CASPT2, keeping the geometry of the ligands fixed, are given in Table 6; this distance becomes shorter with a more negative ligand and with a

Table 6. Optimized distance, d, between Ln and the center of the ligand [Å]; J of the ground term; M_J of the ground state; α_J; sign of $\alpha_J B_2^0$; and CFPs [cm^{-1}] fitted on the $2J+1$ lowest SO-CASSCF energies and corresponding root-mean-square deviations (RMSDs).

	d	J	$\lvert M_J^{GS}\rvert$	α_J	$\alpha_J B_2^0$	B_2^0	B_4^0	B_6^0	RMSD
DyCp	2.36	15/2	15/2	−0.006	−	1303	23	−67	2.6
HoCp	2.34	8	7	−0.002	−	1331	12	−79	0.9
ErCp	2.32	15/2	7/2	0.003	+	1316	19	−154	0.5
TmCp	2.31	6	0	0.01	+	1315	15	−75	1.1
DyBz	2.45	15/2	15/2	−0.006	−	973	14	−48	1.3
HoBz	2.43	8	7	−0.002	−	992	12	−54	0.5
ErBz	2.43	15/2	7/2	0.003	+	984	14	−97	0.2
TmBz	2.43	6	0	0.01	+	977	13	−46	0.5
DyCOT	2.02	15/2	9/2	−0.006	+	−498	−280	38	1.6
HoCOT	2.01	8	4	−0.002	+	−506	−251	25	0.5
ErCOT	1.99	15/2	15/2	0.003	−	−520	−235	43	0.1
TmCOT	1.98	6	6	0.01	−	−510	−221	16	0.7

smaller ionic radius of the lanthanide, as expected. The SO-CASSCF energies of the $2J+1$ ground manifold are shown in Figure 5; the quantification axis is along the C_n axis. The energies show a monotonic variation with $|M_J|$ from 0 to 6 for **TmCp**; the order is reversed from 15/2 to 1/2 for **DyCp** and the gap between two adjacent states increases with $|M_J|$. The energies are more tangled for **HoCp** and **ErCp**, with the states with the largest values of $|M_J|$ lying at the bottom and top of the spectrum, respectively. The **LnBz** series has the same spectra as those for **LnCp**, within a smaller scale. For **DyCOT** and **TmCOT**, the dependence on $|M_J|$ is more intricate; states with the highest value of $|M_J|$ lie highest for **DyCOT** and **HoCOT** and lowest for **ErCOT** and **TmCOT**.

In axial symmetry, the CF Hamiltonian of Equation (3) reduces to Equation (9):

$$V_{ax}^{CF} = \alpha_X B_2^0 \hat{O}_2^0(X) + \beta_X B_4^0 \hat{O}_4^0(X) + \gamma_X B_6^0 \hat{O}_6^0(X) \quad (9)$$

Only three CFPs have to be determined; states with different M_X do not couple, that is, M_X is a good quantum number. According to CFT, α_X, β_X, and γ_X are determined by the metal ion, which determines the values of N, L, and J, whereas the three CFPs B_n^0 depend on the nature and position of the ligands. As shown in the previous section, CFPs for $X=l$, L, and J are very similar (see Table 2). The CFPs fitted on the $2J+1$ lowest SO-CASSCF energies are shown in Table 6 for the three series **LnCp**, **LnBz**, and **LnCOT** (Ln = Dy, Ho, Er, Tm) at their equilibrium distance. The three CFPs fit the energy spectra with negligible RMSDs; they are rather constant in the series, and the decrease in the Ln–ligand distance is rather small. Complexes **LnCp** and **LnBz** have the same ground state for a given Ln and the CFPs are similar with a dominant positive B_2^0. If one neglects the fourth and sixth orders, expressing the Stevens operator in terms of the angular momentum operator, Equation (9) becomes Equation (10)[22]

$$V_{ax}^{CF} = \alpha_X B_2^0 \left(3\hat{X}^2 - X(X+1)\right) \quad (10)$$

and the energy of a $|M_X\rangle$ state is given by Equation (11):

$$E(M_X) = \alpha_X B_2^0 \left(3M_X^2 - X(X+1)\right) \quad (11)$$

According to Equation (11), the sign of the product of $\alpha_X B_2^0$ determines the nature of the ground state: if $\alpha_J B_2^0$ is negative, the ground state (with SOC) is $|M_J| = J$ and the magnetization is axial; conversely, if $\alpha_J B_2^0$ is positive, the ground state for an even number of electrons is $M_J = 0$ and nonmagnetic, whereas for an odd number of electrons it is $|M_J| = 1/2$, which is a doublet with axial magnetization. It follows that, along the lanthanide series, in the case of a positive and constant B_2^0 and given the fact that α_J is positive in the first and third quarters of the series (Ce–Nd, Tb–Ho) and negative in the other quarters (Pm–Sm, Er–Yb), Equation (11) predicts 1) a ground state with axial magnetization for Ce–Nd and Tb–Ho, 2) a nonmagnetic ground state for Pm and Tm, and 3) planar magnetization for Sm, Er, and Yb. This rule is fulfilled if $\alpha_J B_2^0 < 0$ (almost in the case of **HoCp** and **HoBz**) because the energy gaps between adjacent states are larger. For $\alpha_J B_2^0 > 0$, the ground state is

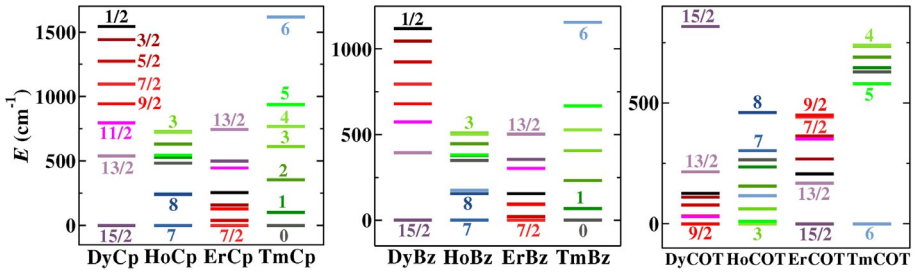

Figure 5. The SO-CASSCF energies of the $2J+1$ lowest states. Zero is the ground state; states are labeled and colored after $|M_J|$.

often an intermediate value of $|M_J|$ due to the fourth-order term, except for Tm for which α_J is the largest, and consequently, the qualitative role of the second-order term is enhanced. The spectra in Figure 5 are more tangled for all Ho and Er complexes because in those cases the values of α_J are smaller than those for Dy and Tm. In the **LnCOT** series, B_2^0 is negative and B_4^0 is more important. Due to this latter term, the spectra of **DyCOT** and **TmCOT** are not as spread as those for **DyCp** and **TmCp**; the two states with the largest $|M_J|$ are well separated from the other ones. To summarize, there is an "up–down" symmetry between Dy/Tm and Ho/Er due to the change in sign of α_J. Complexes with Cp^- and Bz have similar spectra dominated by a large positive B_2^0, whereas with COT^{2-} the spectra are reversed because B_2^0 is negative, and they are more intricate because of the importance of B_4^0.

We showed in the previous section that the many-electron problem may be reduced to a discussion of the energies of the 4f orbitals. Figure 1 shows that the relative energies of the 4f orbitals do not depend on the cation and Figure 2 shows that the energies of the many-electron states deduced from the 4f energies retrieve the main features of SO-CASSCF energies and, in particular, that the nature of the ground state is correctly predicted. For brevity, in the remainder of this section, the discussion is restricted to the ordering of the 4f orbitals in the Dy^{III} complexes.

As seen in Figure 1 and from the sign of B_2^0, the effect of the Cp^- and Bz ligands is qualitatively similar and opposite to that of COT^{2-}; this shows that the total charge of the ligand does not play the key role. To unravel electrostatic and covalent contributions, the ligands must be described by a distribution of point charges. The first level of the model is to distribute the total charge, q, of the ligand uniformly on the n carbon atoms. The electric quadrupole moment, Q_{zz}, of two charges, q, uniformly distributed on two regular n-sided polygons with a radius r, perpendicular to the z axis and separated by a distance 2 d, is given by Equation (12):

$$Q_{zz} = q(-8r^2 + 16d^2) \qquad (12)$$

with a negative value of q, Q_{zz} is positive for an oblate environment with $d/r < 1/\sqrt{2}$ and negative for a prolate one. The ratio d/r equals 1.97, 1.76, and 0.90 in **DyCp**, **DyBz**, and **DyCOT**, respectively; all values are larger than $1/\sqrt{2}$, but the last one is much closer. Although q equals -1 and -2 for Cp^- and COT^{2-}, respectively, it should be 0 for Bz. According to this first model, Cp^- and COT^{2-} generate a B_2^0 of the same sign, whereas no field would be generated for Bz. Warren showed that this simple ionic model led to a positive B_2^0.[68]

Due to the symmetry of the complexes, the first terms of the multipole expansion of the electrostatic field generated by the ligands reduce to the charge, quadrupole, and hexadecapole moments. To be meaningful, the charge distribution that models the ligands has to generate an electrostatic field as close as possible as the one generated by the "chemical" ligands, and consequently, reproduce the first multipole moments. We chose a three-layer charge scheme (see Figure 6), with a layer of positive point charges, q_2, at the actual positions of the carbon atoms and two layers of negative point charges, q_1 and q_3, placed ± 1 Å above and below the positive charges as a simple representation of the aromatic molecule, with a shell of positive nuclei between the two rings of electron currents. The sum of charges is set to the total charge q, and q_1, q_2, and q_3 are optimized to give the same quadrupole and hexadecapole moments as that of the ligands in the presence of a $+3$ charge at the position of the lanthanide. The $+3$ central charge polarizes the ligands. It should be noted that the quadrupole moment, Q_{zz}, of the dimer of benzene (Bz_2) separated by $2d = 2.9$ Å is negative, but becomes positive if a $+3$ charge is placed between the two benzene molecules. A $+3$ charge or a Dy^{III} atom, however, leads to almost identical multiple moments. The parameters of the charge distribution are given in Table 7. For the three ligands, the charge of the inner negative layer (q_1) is larger than the charge of the outer layer (q_3), which mimics polarization effects. As long as the multipole moments are kept the same, the results do not depend on the distance between the layers. The shape of the polygon does not play a role either: for a given radius r and charge q, the results are almost identical for penta-, hexa-, or octagons.

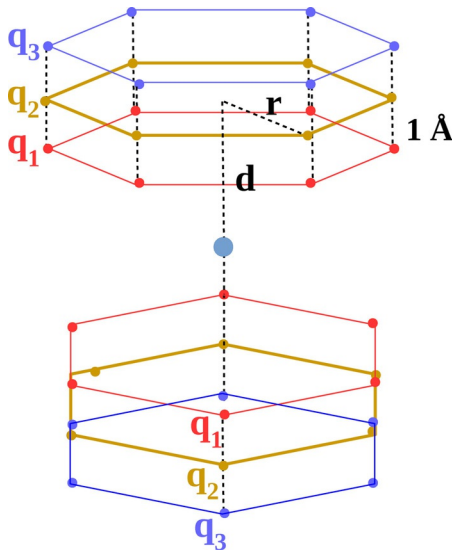

Figure 6. Three-layer charge distribution for Bz_2.

Table 7. Parameters for the three-layer charge distribution and ab initio values of the traceless quadrupole [D Å] and hexadecapole [D Å^3] moments. Distances are given in Å.

	DyCp	DyBz	DyCOT
r	1.201	1.391	1.825
d	2.36	2.45	2.02
q_1	−0.41	−0.42	−0.25
q_2	0.36	0.62	0.13
q_3	−0.15	−0.2	−0.13
Q_{zz}	−12.2	31.2	−37.3
H_{zzzz}	−379.2	−618.6	−66.6
H_{xxyy}	−47.4	−77.3	−8.3
H_{xxzz}	189.6	309.3	33.3

As in the previous section, the complex is built step by step: 1) From a CF, for which the 4f orbitals are in the electrostatic potential of the three layers of charges (denoted **CF4f**). 2) The CASSCF calculation of a Dy^{III} cation described with a basis set (TZP) and the ligands by the three layers of point charges (denoted **CF**). 3) The CASSCF calculation with basis sets on all atoms, but with a restricted TZP* basis on the central Dy^{III} cation without any 6p and 5d orbitals, to avoid any charge donation from the ligands into those orbitals (denoted **no5d6p**). 4) Finally, the CASSCF calculation with complete basis sets on all atoms (denoted **tot**). The energy of the 4f orbitals for these four levels of calculation are represented in Figure 7 at the equilibrium distance and the corresponding CFPs are given in Table 10, below. Orbitals are denoted according to their value of $|m_l|$. Complex **CF4f** leads to opposite ordering of the 4f orbitals with Cp^- and COT^{2-} and the splitting is very small with Bz; this does not follow the quadrupole moments (see Table 7), which are both negative for the former ones and positive and non-negligible for the latter. With COT^{2-}, the CF is dominated by the layer of charges, q_1, closest to the cation for which $r/d_1 < \sqrt{2}$ and, consequently, this layer generates a quadrupole moment opposite to that of Cp^-. For Bz, even if the quadrupole moment is non-negligible due to polarization, the CF is negligible. For the three complexes, the inclusion of orbitals of the cation other than 4f leads to a reduction of 40–50% of all CFPs due to screening by the filled 5s and 5p orbitals and polarization, as in $PrCl_3$.

We designate the difference between **tot** and **CF** values, which include combined effects of bonding, charge donation, and polarization, as the covalent contribution to CFPs. This contribution is split in two: the difference between **no5d6p** and **CF**, which reflects the covalent bonding of the 4f orbitals with the orbitals of the ligands (denoted **covf**), and the difference between **tot** and **no5d6p** (denoted **CTpd**), which describes the effect of electron transfer from the ligands into the empty orbitals of the cation. This latter technique was used to analyze the involvement of 6d orbitals in the bonding of actinide complexes.[69] The π orbitals of the ligands are denoted as $\pi^{\pm}_{|m_l|}$, according to their symmetry; the irreducible representations (irreps) spanned by these orbitals are given in Table 8 and ± denotes the ± combination of the orbitals of the two ligands. According to ligand field theory, metal orbitals with the symmetry of the occupied (unoccupied) orbitals of the ligands are destabilized (stabilized) as antibonding (bonding). Cp^- and

Table 8. Irreducible representations spanned by the orbitals of the metal and the π orbitals of the ligands.

	D_{5d}				D_{6d}				D_{8h}			
$\|m_l\|$	p	d	f	πL	p	d	f	πL	p	d	f	πL
0	A_{2u}	A_{1g}	A_{2u}	$A_{1g} \oplus A_{2u}$	B_2	A_1	B_2	$A_1 \oplus B_2$	A_{2u}	A_{1g}	A_{2u}	$A_{1g} \oplus E_{1u}$
1	E_{1u}	E_1	E_{1u}	$E_{1g} \oplus E_{1u}$	E_1	E_5	E_1	$E_1 \oplus E_5$	E_{1u}	E_{1g}	E_{1u}	$E_{1g} \oplus E_{1u}$
2		E_{2g}	E_{2u}	$E_{2g} \oplus E_{2u}$		E_2	E_4	$E_4 \oplus E_2$		E_{2g}	E_{2u}	$E_{2g} \oplus E_{2u}$
3			E_{2u}				E_3	E_3			E_{3u}	$E_{3g} \oplus E_{3u}$
4												$B_{1g} \oplus B_{2u}$

Bz both have a $(\pi_0)^2(\pi_1)^4$ configuration, with a LUMO of symmetry π_2, and Bz has a vacant π_3. Contribution **covf** leads to a destabilization of f_1 and f_0 and to a stabilization of f_2 and f_3; in **DyCp**, f_3 is destabilized because both f_2 and f_3 span the same irrep as that of the vacant π_2, and in **DyBz** f_3 is more stabilized than f_2 due a strong hybridization of π_3 with the σ orbitals of Bz. COT^{2-} has a $(\pi_0)^2(\pi_1)^4(\pi_2)^4$ configuration with vacant π_3 and π_4 orbitals: the f_2 are destabilized by the π_2^- and the f_3 are stabilized by the π_3^- orbitals.

The main effect of **covf** is the destabilization of the f_3 orbital in **DyCOT**. Electron transfer occurs mostly from the occupied π orbitals of the ligands towards the cation orbitals with the same symmetry. It may be analyzed with the Mulliken population of the 5d and 6p orbitals of the cation given in Table 9.

Table 9. Mulliken populations of the 5d and 6p orbitals at equilibrium distance and with full basis set.

	DyCp		DyBz		DyCOT	
$\|m_l\|$	5d	6p	5d	6p	5d	6p
0	0.08	0.21	0.07	0.24	0.4	0.07
1	0.83	0.33	0.72	0.26	0.40	0.24
2	0.02	–	0.01	–	0.68	–

The donation is the largest into the 5d orbital with the symmetry of the HOMO of the ligands, namely, $5d_1$ in **DyCp** and **DyBz**, and $5d_2$ in **DyCOT**. Donation into $6p_0$ and $6p_1$ for the former, and into $5d_1$ and $6p_1$ for the latter, is also important. These populations are similar, although arising from π and δ interactions for $5d_1$ and $5d_2$, respectively, but due the short metal–ligand distance *d* in **DyCOT**, the δ interactions may be important. Excess electron density on the cation arising from

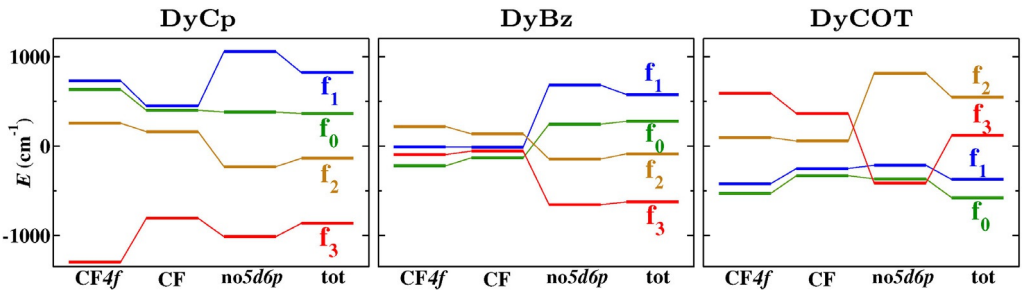

Figure 7. Energies of the 4f orbitals obtained with 4f + *Q* (**CF4f**), TZP + *Q* (**CF**), TZP + DZP* (**no5d6p**), and TZP + DZP (**tot**) at equilibrium distance. *Q* denotes the charge distribution given in Table 7. Zero is taken as the average of the seven energies. Orbitals are labeled and colored after $|m_l|$.

this charge transfer is not isotropic and, in the case of the $5d_2$ orbitals, increases the density in the equatorial region. Because the $4f_3$ orbitals also lie in the equatorial plane, electron–electron repulsion between the $5d_2$ electron density is largest with the $4f_3$ electron density and this leads to a destabilization of these orbitals.

The partition between covalent bonding and charge transfer is somewhat arbitrary: Mulliken charges are not quantitative and the avoidance of charge transfer by removing some orbitals from the basis sets has some side effects. However, the aim of this work is to unravel general trends. The CFPs determined at each step are given in Table 10. B_2^0 are large and opposite for **DyCp** and **DyCOT** due to the position of the first layer of charges, which generates opposite quadrupolar moments in the two systems. B_2^0 vanishes in **DyBz** through compensation from the other layers, the total charge of which vanishes. The screening of 4f leads to a reduction of 40–50% of all CFPs. Bonding with 4f gives a positive contribution to B_2^0 because f_0 and f_1 are destabilized and f_3 is stabilized; this means that it adds to the **CF** contribution for **DyCp**, annihilates it for **DyCOT**, and is the leading contribution for **DyBz**. Charge transfer counterbalances the 4f bonding and the total B_2^0, with covalent effects rather close to that of the CF for **DyCp** and **DyCOT**. The effect is larger for higher order CFPs and the most qualitative effect is the change of ordering between f_2 and f_3 in **DyCOT**.

Table 10. CFPs deduced from the 4f energies for the sandwich complexes at equilibrium geometry.

	DyCp			DyBz			DyCOT		
	B_2^0	B_4^0	B_6^0	B_2^0	B_4^0	B_6^0	B_2^0	B_4^0	B_6^0
CF4f	1777	−164	−21	1	−133	−7	−947	−48	12
CF	1103	−102	−11	−3	−82	−3	−577	−29	5
no5d6p	1607	41	−144	1037	25	−92	123	−442	56
tot	1339	15	−100	966	7	−67	−511	−299	35

The effect of metal–ligand distance for the different contributions is shown in Figure 8. There is a reversal of the ordering of the **CF** contribution, according to Equation (12); the charge distribution is oblate at small distances d and prolate at large ones. The reversal point occurs at shorter distance for Cp^- due to the smaller radius r of the ligands, and the levels are more grouped for COT^{2-} due the small value of the hexadecapole moment. It should be noted that **CF** is small for **DyBz** in the equilibrium region, but much larger at smaller distances. Contribution **covf** decreases exponentially, as does the overlap between the 4f and π orbitals of the ligands. Orbitals f_2 and f_3 cross in **DyCp** because they span the same irrep and the hybridization varies with the distance. The **CTpd** contribution is almost constant at this range of distance because it arises from overlap between the orbitals of the ligands and 5d and 6p, which are more diffuse than that of 4f. Thus, the final dependence of the 4f energies on the distance is neither of the CFs because there is no crossing, nor ordering of the covalent effect.

The effects of Cp^- and Bz are opposite to that of COT^{2-}, in the sense that, if the first two lead to planar magnetization, the last one leads to an axial one and conversely. This is due to opposite signs of B_2^0, and consequently, to a reverse ordering of the 4f orbitals. The environment of the **LnCp** and **LnBz** complexes is prolate because of both the smaller radii of the ligands and longer bonding distance (due to the smaller charge of the ligands). The environment is more compressed with COT^{2-}, which has a larger radius and a charge of −2. The CF contribution is indeed opposite for Cp^- and COT^{2-}, and vanishes in the case of Bz. The covalent contributions in the case of Cp^- and Bz ligands differ from that of COT^{2-} due to the nature of the frontier orbitals; this impacts mostly on the $4f_2$ orbitals, which are stabilized by a bonding interaction in the **LnCp** and **LnBz** complexes and destabilized by an antibonding interaction in the **LnCOT** complex. Moreover, charge transfer into the $5d_2$ orbitals from COT^{2-} destabilizes the $4f_3$ orbitals of the Ln by indirect electron–electron repulsion. Covalent effects give the main contribution in **LnCp** complexes and reverse the ordering of $4f_2$ and $4f_3$ orbitals in **LnCOT** ones. According to Figure 8, CF and covalent contributions are of the same order of magnitude in these sandwich complexes and must be taken into account to fully understand splitting of the Stark levels.

Conclusions

CFT is based on the idea that the Stark levels of the free lanthanide ion are split by the electrostatic field generated by the ligands. Early on, it was understood that the electrostatic approach was not quantitative and theory has been used as a frame, the parameters of which, the CFPs, were fitted to experimental data. This theory has been extensively used, and still is, and permits the description of the lanthanide complexes by means of a reduced number of parameters. For a decade, lanthanide complexes have been widely used for the study of single-molecule magnets. To optimize the magnetic properties, the design of molecules with a large magnetic moment is necessary, and understanding of the factors that determine the nature of the ground state is of prime importance. Herein, we aimed at unraveling the different physical contributions to the CFPs. To achieve this goal, we chose symmetrical molecular systems to reduce the number of CFPs and avoid any overparametrization: an ionic crystal of $PrCl_3$ and a series of sandwich complexes in which the presence of aromatic ligands led to larger covalent effects and a delocalization of the charge that made the modeling by point charges less evident.

First, we discussed the independent electron approximation. CFPs determined from one-electron (orbital) energies and from many-electron wave functions compare well because two-electron interactions do not vary strongly within a $(4f)^N$ configuration because of the semicore nature of the 4f orbitals. Furthermore, splitting of the 4f orbitals remains small enough, such that it does not affect the composition of the many-electron wave function from the free ion obtained by coupling the angular momenta. Thus, the relative energies of the $2J+1$ terms arising from the free-ion ground term, $^{2S+1}L_J$, derive mostly from the relative energies of the seven 4f orbitals. This reduces

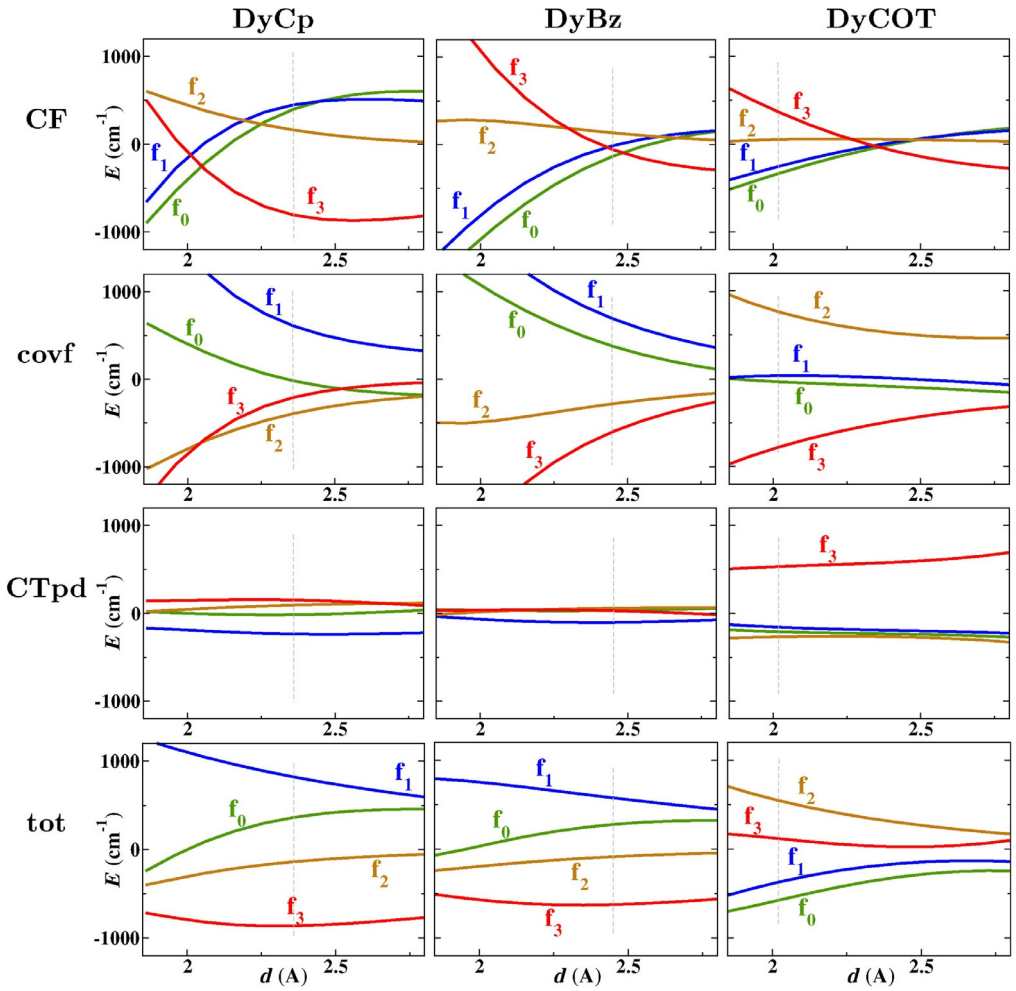

Figure 8. Energies of the 4f orbitals as a function of Ln–ligand distance. **CF**: TZP + Q; **covf**: **CF**−**no5d6p**; **CTpd: no5d6p**−**tot**; **tot**: full basis set. Zero is taken as the average of the seven energies at each distance, and the orbitals are labeled and colored after $|m_l|$. The vertical line denotes the equilibrium distance.

the many-electron problem to the discussion of the ordering of the 4f orbitals. It was similarly showed recently that the ordering of the 3d orbital energies determined the zero field splitting in a quasi-octahedral Ni^{II} complex.[70]

Second, the step by step construction of the $PrCl_3$ crystal shows that 1) the electrostatic field generated by the ligands is shielded about 40% by the outermost filled shells of the cation, 2) the covalency plays an important role by decreasing B_2^0 by 50% and giving rise to an important B_6^6 term due to the anisotropy of bonding interactions, and 3) part of the crystal out of the $[PrCl_9]^{6-}$ cluster plays a non-negligible role and impacts on the CFPs by 15%. In the case of an ionic crystal, the electrostatic picture is qualitatively correct, but covalency has to be taken into account for quantitative results.

Finally, three series of sandwich complexes were considered. Depending on both the nature of the central cation and the ligands, magnetization of the ground state is either axial or equatorial. A three-layered charge distribution was proposed to model the electrostatic field generated by the ligands; the charges were fitted to reproduce the multipole moments of the actual ligands in the presence of a central +3 charge. This model permits the evaluation of the CF contribution to the CFPs. As for $PrCl_3$, the electrostatic field generated by the ligands is shielded by about 40% by the external filled orbitals of the metal. In the case of the neutral ligand Bz, the CF contribution is small and it is opposite for prolate $[Ln(Cp)_2]^+$ and oblate $[Ln(COT)_2]^-$. The covalent contribution to CFPs is of the same order of magnitude as that of the CF one: the main part is due to the interaction of 4f with the orbitals of the ligands, mostly the π system, but sometimes hybridized with σ orbitals. In the case of $[Ln(COT)_2]^-$, charge transfer from the ligands to the 5d orbitals plays an important role on the relative energies of the 4f orbitals due to electron–electron interactions. Recent analysis of X-ray absorption spectra in Ln_2O_3 and $[LnCl_6]^{x-}$ complexes have provided evidence of the role of the 5d orbitals in bonding, but revealed a marginal role of the 4f orbitals.[71,72] This tiny covalent interaction between the 4f orbitals and the ligands does not affect the chemical properties, but, regardless of how small it might be, plays a quantitative, even qualitative, role in the splitting of the 4f orbitals, and consequently, impacts on the magnetic properties. This work shows that, as is sometimes the case in transition-metal complexes[73] and recently shown for actinide complexes,[74] CF and covalency are closely entangled.

Computational Details

First-principles calculations were performed with the MOLCAS78 suite of programs.[75] First, a SF-CASSCF calculation was performed.[76] SOC is included by a state interaction with the restricted active space state interaction (RASSI) method.[77] Scalar relativistic effects were taken into account by means of the Douglas–Kroll–Hess transformation[78] and SO integrals were calculated using the atomic mean-field integrals (AMFI) approximation.[79] The *g* factors were calculated, as described in reference [80].

For the $PrCl_3$ crystal, calculations were performed by using the crystallographic structure. $[PrCl_9]^{6-}$ was described with ANO-RCC basis sets of TZP quality. This cluster was embedded in point charges (+3 for Pr, −1 for Cl) within a radius of 8 Å positioned at the crystallographic sites. The active space consisted of two electrons spread over the seven 4f orbitals. The SOC was calculated with 21 and 28 spin triplet and singlet states. In the step by step procedure, calculations were performed without spin singlets in the SOC step, without embedding, replacing Cl^- by either point charges $Q=-1$ or point charges with ECPs, and with a minimal basis set or a single 4f Slater on Pr, as specified in the text.

For $[Ln(\eta^n\text{-}C_nH_n)_2]^q$ complexes, the geometry of the ligands was optimized by using DFT-B3LYP[81,82] with the NWChem 6.1 package[83] and a cc-pVTZ basis sets[84] (see Table 11). Frequency analysis was performed afterwards to ensure that real minima were obtained. The Ln–cycle distance was optimized by using CASPT2[85] by keeping the geometry of the ligands frozen. Ln, C, and H atoms were described with ANO-RCC basis sets of TZP and DZP quality. In a lanthanide with configuration $4f^N$ a CAS(N,7) is used with 21 sextets (Dy), 35 quintets (Ho), 35 quartets (Er), or 2 triplets (Tm) at the SO step. For the step-by-step procedure, ligands were replaced by three layers of point charges, and the Ln atom was described by either a 8s4p2d3f2g1h basis set (denoted TZP*) or a single 4f Slater (CFf).

Table 11. Optimized distances [Å] for $C_nH_n^q$.

	Cp^-	Bz	COT^{2-}
r_{C-C}	1.412	1.391	1.397
r_{C-H}	1.083	1.082	1.102

Acknowledgements

We thank Ria Broer and Remco W. A. Havenith for fruitful discussions. R.A. and H.Z. would like to acknowledge the Erasmus Mundus programme of the European Union for financial support, and J.A. the support of the US Department of Energy, Office of Basic Energy Sciences, Heavy Element Chemistry program, under grant DE-SC0001136, for our collaborative work and University of Toulouse 3 for a visiting professor fellowship in May 2013.

Conflict of interest

The authors declare no conflict of interest.

Keywords: ab initio calculations · bond theory · crystal field effects · lanthanides · ligand effects

[1] D. J. Newman, *Adv. Phys.* **1971**, *20*, 197.
[2] H. Bethe, *Ann. Phys.* **1929**, *395*, 133.
[3] J. H. Van Vleck, *J. Chem. Phys.* **1935**, *3*, 807.
[4] G. Racah, *Phys. Rev.* **1949**, *76*, 1352.
[5] K. W. H. Stevens, *Proc. Phys. Soc. London Sect. A* **1952**, *65*, 209.
[6] B. R. Judd, *Proc. R. Soc. London Ser. A* **1955**, *232*, 458.
[7] J. S. Griffith, L. E. Orgel, *Rev. Chem. Soc.* **1957**, *11*, 381.
[8] C. J. Ballhausen, *Introduction to Ligand Field Theory*, McGraw-Hill, New-York, **1962**.
[9] H. Schilder, H. Lueken, *J. Magn. Magn. Mater.* **2004**, *281*, 17 – 26.
[10] N. F. Chilton, R. P. Anderson, L. D. Turner, A. Soncini, K. S. Murray, *J. Comput. Chem.* **2013**, *34*, 1164 – 1175.
[11] J. D. Rinehart, J. R. Long, *Chem. Sci.* **2011**, *2*, 2078 – 2085.
[12] J. J. Baldoví, J. J. Borrási-Almenar, J. M. Clemente-Juan, E. Coronado, A. Gaita-Ariño, *Inorg. Chem.* **2012**, *51*, 13705.
[13] J. J. Baldoví, J. M. Clemente-Juan, E. Coronado, A. Gaita-Ariño, *Inorg. Chem.* **2014**, *53*, 11323 – 11327.
[14] N. F. Chilton, D. Collison, E. J. L. McInnes, R. E. P. Winpenny, A. Soncini, *Nat. Commun.* **2013**, *4*, 2551.
[15] L. E. Roy, N. J. Bridges, L. R. Martin, *Dalton Trans.* **2013**, *42*, 2636 – 2642.
[16] W. A. Rabanal-León, D. Páez-Hernández, R. Arratia-Pérez, *Phys. Chem. Chem. Phys.* **2014**, *16*, 25978 – 25988.
[17] W. Ji, W. Xu, W. H. E. Schwarz, S. Wang, *J. Comput. Chem.* **2015**, *36*, 449 – 458.
[18] T. Gupta, G. Velmurugan, T. Rajeshkumar, G. Rajaraman, *J. Chem. Sci.* **2016**, *128*, 1615 – 1630.
[19] T. J. Duignan, J. Autschbach, *J. Chem. Theory Comput.* **2016**, *12*, 3109 – 3121.
[20] D. Aravena, M. Atanasov, F. Neese, *Inorg. Chem.* **2016**, *55*, 4457 – 4469.
[21] L. Ungur, L. F. Chibotaru, *Chem. Eur. J.* **2017**, *23*, 3708 – 3718.
[22] A. Abragam, B. Bleaney, *Electronic Paramagnetic Resonance of Transition Ions*, Clarendon Press, Oxford, **1970**.
[23] M. T. Hutchings, D. K. Ray, *Proc. Phys. Soc. London* **1963**, *81*, 663.
[24] D. K. Ray, *Proc. Phys. Soc. London* **1963**, *82*, 47.
[25] A. K. Raychaudhuri, D. K. Ray, *Proc. Phys. Soc. London* **1967**, *90*, 839.
[26] M. Faucher, D. Garcia, *J. Less-Common Met.* **1983**, *93*, 31 – 44.
[27] R. E. Watson, A. J. Freeman, *Phys. Rev.* **1964**, *133*, A1571.
[28] R. M. Sternheimer, *Phys. Rev.* **1966**, *146*, 140.
[29] R. M. Sternheimer, M. Blume, R. F. Peierls, *Phys. Rev.* **1968**, *173*, 376.
[30] K. Rajnak, B. G. Wybourne, *J. Chem. Phys.* **1964**, *41*, 565.
[31] J. C. Morrison, P. R. Fields, W. T. Carnall, *Phys. Rev. B* **1970**, *2*, 3526.
[32] H. S. Jarrett, *J. Chem. Phys.* **1959**, *31*, 1579 – 1585.
[33] C. K. Jørgensen, R. Pappalardo, H. H. Schmidtke, *J. Chem. Phys.* **1963**, *39*, 1422.
[34] R. E. Watson, A. J. Freeman, *Phys. Rev.* **1967**, *156*, 251.
[35] C. E. Schäffer, C. K. Jørgensen, *Mol. Phys.* **1965**, *9*, 401 – 412.
[36] D. J. Newman, B. Ng, *Rep. Prog. Phys.* **1989**, *52*, 699 – 763.
[37] D. H. Templeton, C. H. Dauben, *J. Am. Chem. Soc.* **1954**, *76*, 5237.
[38] B. Morosin, *J. Chem. Phys.* **1968**, *49*, 3007.
[39] E. V. Sayre, K. M. Sancier, S. Freed, *J. Chem. Phys.* **1955**, *23*, 2060.
[40] C. A. Hutchison, Jr., E. Wong, *J. Chem. Phys.* **1958**, *29*, 754.
[41] B. R. Judd, *Proc.-R. Soc. Edinburgh, Sect. A: Math. Phys. Sci.* **1957**, *156*, 45.
[42] J. S. Margolis, *J. Chem. Phys.* **1961**, *35*, 1367.
[43] R. Sarup, M. H. Crozier, *J. Chem. Phys.* **1965**, *42*, 371.
[44] M. M. Ellis, D. J. Newman, *J. Chem. Phys.* **1967**, *47*, 1986.
[45] S. S. Bishton, M. M. Ellis, D. J. Newman, J. Smith, *J. Chem. Phys.* **1967**, *47*, 4133.
[46] M. M. Ellis, D. J. Newman, *J. Chem. Phys.* **1968**, *49*, 4037.
[47] M. M. Curtis, D. J. Newman, G. E. Stedman, *J. Chem. Phys.* **1969**, *50*, 1077.
[48] M. Mater. Salleh, G. M. Copland, *J. Phys. C* **1978**, *11*, L777.
[49] F. Gendron, D. Páez Hernàndez, F. P. Notter, B. Pritchard, H. Bolvin, J. Autschbach, *Chem. Eur. J.* **2014**, *20*, 7994.
[50] M. N. Bochkarev, *Chem. Rev.* **2002**, *102*, 2089 – 2118.
[51] R. J. Strittmatter, B. E. Bursten, *J. Am. Chem. Soc.* **1991**, *113*, 552 – 559.
[52] J. C. Green, D. Hohl, N. Roesch, *Organometallics* **1987**, *6*, 712 – 720.

[53] F. G. N. Cloke, *Chem. Soc. Rev.* **1993**, *22*, 17 – 24.
[54] G. Hong, F. Schautz, M. Dolg, *J. Am. Chem. Soc.* **1999**, *121*, 1502 – 1512.
[55] Y. Lei, L. Wu, B. R. Sohnlein, D. S. Yang, *J. Chem. Phys.* **2012**, *136*, 204311.
[56] Y. Liu, S. Kumari, M. Roudjane, S. Li, D. S. Yang, *J. Chem. Phys.* **2012**, *136*, 134310.
[57] M. D. Walter, C. H. Booth, W. W. Lukens, R. A. Andersen, *Organometallics* **2009**, *28*, 698.
[58] K. Hodgson, F. Mares, D. F. Starks, J. A. Streitwieser, *J. Am. Chem. Soc.* **1973**, *95*, 8650.
[59] J. J. Le Roy, L. Ungur, I. Korobkov, L. Chibotaru, M. Murugesu, *J. Am. Chem. Soc.* **2014**, *136*, 8003.
[60] F. Ferraro, C. Aparecida Barboza, R. Arratia-Pérez, *J. Phys. Chem. A* **2012**, *116*, 4170.
[61] N. Rösch, A. J. Streitwieser, *J. Am. Chem. Soc.* **1983**, *105*, 7237.
[62] D. W. Clack, K. D. Warren, *J. Organomet. Chem.* **1976**, *122*, C28.
[63] A. Kerridge, R. Coates, N. Kaltsoyannis, *J. Phys. Chem. A* **2009**, *113*, 2896.
[64] F. Gendron, B. Pritchard, H. Bolvin, J. Autschbach, *Dalton Trans.* **2015**, *44*, 19886.
[65] K. R. Meihaus, J. R. Long, *J. Am. Chem. Soc.* **2013**, *135*, 17952.
[66] J. J. Le Roy, M. Jeletic, S. I. Gorelsky, I. Korobkov, L. Ungur, L. Chibotaru, M. Murugesu, *J. Am. Chem. Soc.* **2013**, *135*, 3502.
[67] C. A. P. Goodwin, F. Ortu, D. Reta, N. F. Chilton, D. P. Millsi, *Nature* **2017**, *548*, 439 – 442.
[68] K. D. Warren, *Inorg. Chem.* **1975**, *14*, 3095.
[69] H. Bolvin, U. Wahlgren, O. Gropen, C. Marsden, *J. Phys. Chem. A* **2001**, *105*, 10570.
[70] G. Charron, E. Malkin, G. Rogez, L. J. Batchelor, S. Mazerat, R. Guillot, N. Guihéry, A. L. Barra, T. Mallah, H. Bolvin, *Chem. Eur. J.* **2016**, *22*, 16850 – 16862.
[71] M. W. Löble, J. M. Keith, A. B. Altman, S. C. E. Stieber, E. R. Batista, K. S. Boland, S. D. Conradson, D. L. Clark, J. Lezama Pacheco, S. A. Kozimor, R. L. Martin, S. G. Minasian, A. C. Olson, B. L. Scott, D. K. Shuh, T. Tyliszczak, M. P. Wilkerson, R. A. Zehnder, *J. Am. Chem. Soc.* **2015**, *137*, 2506 – 2523.
[72] A. B. Altman, J. I. Pacold, J. Wang, W. W. Lukens, S. G. Minasian, *Dalton Trans.* **2016**, *45*, 9948 – 9961.
[73] H. Bolvin, *Eur. J. Inorg. Chem.* **2010**, 2221.
[74] W. W. Lukens, N. M. Edelstein, N. Magnani, T. W. Hayton, S. Fortier, L. A. Seaman, *J. Am. Chem. Soc.* **2013**, *135*, 10742.
[75] F. Aquilante, L. De Vico, N. Ferré, G. Ghigo, P.-A. Malmqvist, P. Neogrády, T. B. Pedersen, M. Pitonak, M. Reiher, B. Roos, M. Serrano-Andrés, M. Urban, V. Veryazov, R. Lindh, *J. Comput. Chem.* **2010**, *31*, 224.
[76] B. O. Roos, P. R. Taylor, P. E. M. Siegbahn, *Chem. Phys.* **1980**, *48*, 157.
[77] P.-A. Malmqvist, B. O. Roos, B. Schimmelpfennig, *Chem. Phys. Lett.* **2002**, *357*, 230.
[78] B. A. Hess, *Phys. Rev. A* **1986**, *33*, 3742.
[79] B. A. Hess, C. M. Marian, U. Wahlgren, O. Gropen, *Chem. Phys. Lett.* **1996**, *251*, 365.
[80] H. Bolvin, *ChemPhysChem* **2006**, *7*, 1575.
[81] A. Becke, *J. Chem. Phys.* **1993**, *98*, 5648.
[82] C. Lee, W. Yang, R. Parr, *Phys. Rev. B* **1988**, *37*, 785.
[83] M. Valiev, E. J. Bylaska, N. Govind, K. Kowalski, T. P. Straatsma, H. J. J. Van Dam, D. Wang, J. Nieplocha, E. Apra, T. L. Windus, W. A. de Jong, *Comput. Phys. Commun.* **2010**, *181*, 1477 – 1489.
[84] T. H. J. Dunning, *J. Chem. Phys.* **1989**, *90*, 1007.
[85] K. Andersson, P.-A. Malmqvist, B. O. Roos, A. J. Sadlej, K. Wolinski, *J. Phys. Chem.* **1990**, *94*, 5483.

Manuscript received: December 4, 2017
Accepted manuscript online: January 22, 2018
Version of record online: March 8, 2018